Nanoscale Advances

ROYAL SOCIETY OF CHEMISTRY

PAPER

View Article Online
View Journal | View Issue

Cite this: *Nanoscale Adv.*, 2024, **6**, 2319

"Turn-on" and pinhole-free ultrathin core–shell Au@SiO_2 nanoparticle-based metal-enhanced fluorescent (MEF) chemodosimeter for Hg^{2+}†

Ying Cui,‡[ab] Shanji Fan,‡[c] Yunran Zhai,[a] Yingjie Liu,[c] Junhua Li,[b] Jiawen Hu*[a] and Lijia Wang *[d]

This study reports a metal-enhanced fluorescence chemodosimeter for highly sensitive detection of Hg^{2+} ions. Silica-coated Au nanoparticles (Au@SiO_2 NPs) with a pinhole-free 4–5 nm shell were synthesized and functionalized with a monolayer of turn-on fluorescent probes. Compared to other organic fluorescent probes suffering from poor biocompatibility and detection limits, this design of a monolayer of turn-on fluorescent probes immobilized on the Au@SiO_2 NPs with a pinhole-free 4–5 nm shell avoids fluorescence quenching and allows the fluorescent probe within the field of the inner Au NPs to experience metal-enhanced fluorescence. With this design, the chemodosimeter permits fluorescence emission in the presence of Hg^{2+} ions, because they trigger the ring-opening reaction of the fluorescent probe immobilized on the Au@SiO_2 NPs. Additionally, the fluorescent probe is distanced by the thin SiO_2 shell from directly attaching to the metallic Au NPs, which not only avoids fluorescence quenching but allows the fluorescent probe within the long-ranged field of the inner Au NPs to experience metal-enhanced fluorescence. As a result, the detection limit for the chemodosimeter can reach up to 5.0×10^{-11} M, nearly two orders of magnitude higher than that achieved for the free fluorescent probe. We also demonstrate the acquisition of images of Hg^{2+} in HTC116 cells and zebrafish using a simple fluorescence confocal imaging technique. The fluorescence response results for HTC116 cells and zebrafish show that the probes can permeate into cells and organisms. Considering the availability of the many organic fluorescent probes that have been designed, the current designed metal-enhanced fluorescence chemodosimeter holds great potential for fluorescence detection of diverse species and fluorescence imaging.

Received 6th September 2023
Accepted 16th December 2023

DOI: 10.1039/d3na00746d

rsc.li/nanoscale-advances

Introduction

Heavy metal ions in the environment, foods and water have received intensive attention for decades.[1] Among them, Hg^{2+} ions are one of the most toxic ions, which, when accumulated through the food chain, may cause damage to skin, respiratory, and gastrointestinal tissues.[2–4] According to the US Environmental Protection Agency (EPA), 10 nM (2 ppb) is the maximum residue limit of Hg^{2+} allowed in drinkable water.[5] To monitor mercury levels in populations occupationally exposed to mercury, numerous methods have been developed, such as atomic absorption spectroscopy (AAS),[6,7] atomic emission spectroscopy (AES),[8,9] and inductively coupled plasma atomic mass spectrometry (ICP-MS)[10,11] methods. Generally, these methods are more precise than other methods but have the drawbacks of requiring expensive equipment and a time-consuming analysis process.[12,13]

In recent years, fluorescence-based colorimetric chemodosimeters for the detection of Hg^{2+} ions have attracted increasing attention because of their high selectivity, sensitivity, irreversible binding ability, mild reaction conditions (*e.g.*, room temperature), and water solubility.[14,15] In 1992, Chae *et al.* first introduced the term chemodosimeter, which refers to an abiotic molecule that recognizes the analyte and at the same time irreversibly transduces an observable signal.[16] Generally, mechanisms for chemodosimeters can be divided into two main modes: the analyte can react with the chemodosimeter or act as a catalyst.[17] For example, one fluorescence chemodosimeter relies on the binding of Hg^{2+} for the desulfurization of a thioamide to amide to produce fluorescence signals.[18–20]

[a]*Hunan Key Laboratory of Two-Dimensional Materials, Advanced Catalytic Engineering Research Center of the Ministry of Education, College of Chemistry and Chemical Engineering, Hunan University, Changsha 410082, China. E-mail: jwhu@hnu.edu.cn*

[b]*Key Laboratory of Functional Metal-Organic Compounds of Hunan Province, College of Chemistry and Materials Science, Hengyang Normal University, Hengyang, 421001, PR China*

[c]*Department of Breast and Thyroid Surgery, The First Affiliated Hospital, Hengyang Medical School, University of South China, Hengyang 421000, China*

[d]*Children's Hospital, Zhejiang University School of Medicine, National Clinical Research Center for Child Health, National Children's Regional Medical Center, Hangzhou, Zhejiang 310052, China. E-mail: wanglijia@zju.edu.cn*

† Electronic supplementary information (ESI) available. See DOI: https://doi.org/10.1039/d3na00746d

‡ Co-first authors.

Because the fluorescence intensity determines the sensitivity of a fluorescent probe, metal-enhanced fluorescence (MEF) has been widely used to enhance the intensity of the fluorescence.[21,22] Surface plasmon resonance is the light-induced of collective oscillation of free electrons in a metal, and thus generates a very strong electromagnetic field that can improve the fluorescence intensity.[23,24] This phenomenon is called metal-enhanced fluorescence (MEF) and has been reported for various organic fluorophores[25,26] and quantum dots[27,28] in proximity to gold or silver substrates or other metal nanostructures. It has also been found that metal nanoparticles (NPs) can affect fluorescence intensity. This effect mostly depends on the distance between the metal nanostructures and fluorophores; too-great proximity results in quenching, while separation by several nanometers produces enhancement.[29] However, when the distance is too large, the fluorophore will be far from the magnetic field generated by the plasma resonance of the metal nanoparticles, and the fluorescence intensity of the fluorophore will not be affected. Therefore, optimization of fluorophore-metal NP distance is critical for fluorescence enhancement.[30] To date, a great deal of work has been performed using metal NPs deposited on glass,[31] plastics,[32,33] paper[34] or other non-metallic plate substrate surfaces *via* self-assembly,[35] to study the MEF effect on photoluminescent materials. Therefore, it is desirable to fabricate uniform and disperse nanocomposite systems to realize the MEF effect in biological,[36] nanophase electronic,[37] single nanoparticle sensing[38,39] and fluorescence imaging.[40]

Fluorescent chemosensors for Hg^{2+} have been extensively explored, including cyclen,[41] hydroxyquinoline,[42] azine,[43,44] diazatetrathia crown ethers[36] and calixarene.[45] However, many of these sensors suffer from limitations in terms of synthetic difficulty, high cost of starting materials, high detection limits or lack of selectivity towards potential competitors such as copper (Cu^{2+}) and silver (Ag^{+}) due to the similarity of their chemical behavior to that of Hg^{2+}.[46] In addition, two different modes, namely, the "turn-off" mode[47] and "turn-on" mode,[48] have been proposed for optical sensors based on fluorescence. Most of the reported fluorescent sensors have been based on the "turn-off" mode, in which false positive results occur due to other quenchers in real samples.[49] Compared to the traditional "turn-off" mode, the latter approach based on the "turn-on" fluorescence change (quenching recovery) can not only expand the detection range but also increase stability and reduce environmental interferences.[50]

In this study, we developed a facile, highly sensitive and selective chemodosimeter for the detection of Hg^{2+} ions based on MEF. This was accomplished by immobilizing a fluorescent probe on ultrathin SiO_2-shell-coated Au NPs[51] (Au@SiO_2 NPs, where the diameter of the SiO_2 shell was 4–5 nm). With this core–shell type configuration, the plasmon of the inner Au NPs produces long-range electromagnetic fields to enhance the fluorescence emission. Additionally, the ultrathin SiO_2 shell can avoid fluorescence quenching through separating the fluorophore probe from the metal. Furthermore, the fluorescence can be further enhanced *via* optimizing the core size. To demonstrate the feasibility of the MEF-based fluorescence platform, we demonstrated its application for the detection of Hg^{2+} ions. The optimized detection limit achieved was 5.0×10^{-11} M, which was about two orders of magnitude lower than that achieved using the free fluorescent probe (8.5×10^{-9} M) and far lower than the permissible EPA limit for Hg^{2+} ions in drinkable water ($<1.0 \times 10^{-9}$ M). Additionally, this MEF-based fluorescence platform has high selectivity for Hg^{2+} over other metal ions. The proposed strategy opens new avenues to fabricate a sustainable chemodosimeter that affords superior performance in the detection of Hg^{2+} in real environments, such as food samples and even whole cells.

Results and discussion

Scheme 1 shows a schematic illustration of the preparation flow for the fluorophore-labeled Au@SiO_2 probe and detection

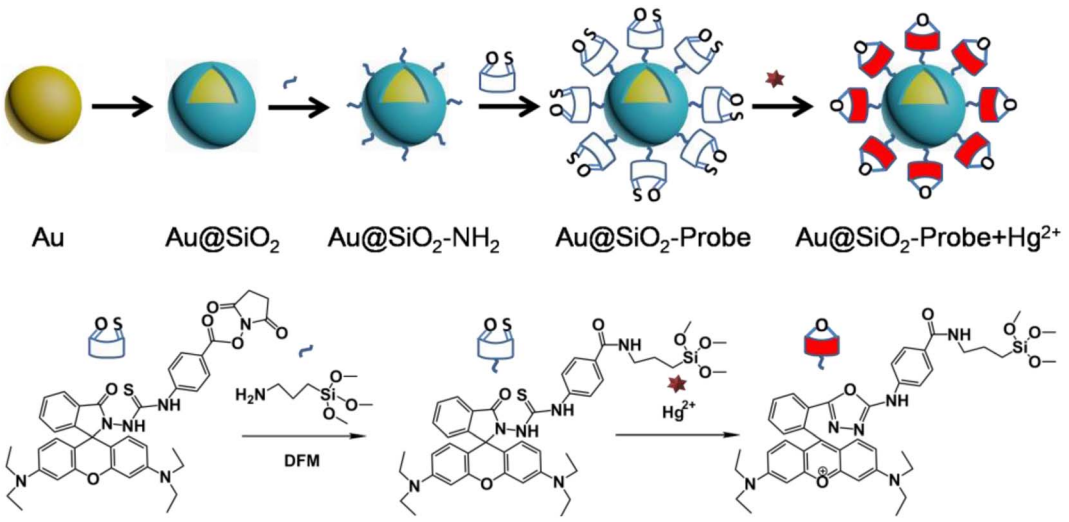

Scheme 1 Schematic illustration of the preparation flow for the fluorophore-labeled Au@SiO_2 NP probe and its detection mechanism for Hg^{2+} ions.

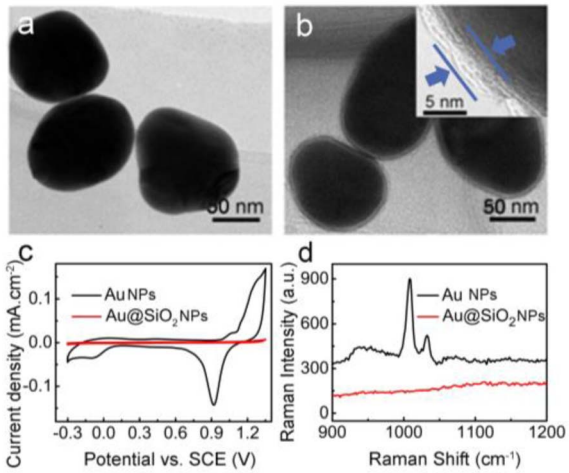

Fig. 1 TEM images for the (a) 80 nm Au NPs and (b) corresponding $Au@SiO_2$ NPs with an external 4–5 nm SiO_2 shell. Inset is a TEM image of $Ag@SiO_2$ NPs to show the silica shell. (c) Cyclic voltammograms of Au NPs and $Au@SiO_2$ in 0.5 M H_2SO_4 solution, scan rate: 0.1 V s^{-1}. (d) Raman spectrum of pyridine; 0.001 M pyridine on Au and $Au@SiO_2$ on a Si wafer, respectively.

mechanism of Hg^{2+} ions. In the absence of Hg^{2+} ions, the fluorophore-labeled $Au@SiO_2$ probe exhibits relatively weak fluorescence emission. In contrast, because of their strong thiophilic affinity, the presence of Hg^{2+} ions can easily open the spirolactam ring (*via* desulfurization reaction) of the fluorophore immobilized on the SiO_2 shell, thereby turning on fluorescence emission.

Silica coating was performed according to the method established by Li *et al.*[51] By carefully controlling reaction parameters such as pH, reaction time, temperature, and the amount of silica source, this method allows coating of the Au NPs with a controlled-thickness SiO_2 shell. Fig. 1 shows the TEM images of the 80 nm Au NPs (a) and the corresponding $Au@SiO_2$ NPs with a 4–5 nm SiO_2 shell (b). Upon silica coating, a thin and uniform SiO_2 shell of ~4–5 nm is clearly seen coating each isolated Au NP. Moreover, the Au NPs supported on the GC electrode show typical electrochemical responses of a polycrystalline Au surface (Fig. 1c), with a wide Au oxide peak initiating at about 1.2 V and a corresponding stripping peak for the Au oxide at 0.9 V. On the contrary, the thin SiO_2 shell completely restrains the formation of the Au oxide peak during the cationic scan and accordingly strips the peak of the Au oxide in the cyclic voltammetry (CV) curve of the $Au@SiO_2$ NPs (Fig. 1c). Therefore, the SiO_2 shell coating is "pinhole-free", as further confirmed by the lack of any discernable SERS peaks for pyridine molecules when immersing the $Au@SiO_2$ NPs in pyridine solution (for details, see Fig. 1d). The naked pure Au NPs show strong SERS peaks because of their easily available surface, which allows the adsorption of the pyridine molecules to experience SERS enhancement. In contrast, the $Au@SiO_2$ NPs do not show any SERS peaks from pyridine, because the SiO_2 shell effectively blocks the pyridine molecules from approaching and adsorbing on the inner Au NPs. This "pinhole-free" SiO_2 shell can thus effectively separate the fluorophore from direct contact with the Au metal underneath, thereby avoiding fluorescence quenching. Conversely, the SiO_2 shell is very thin, so that the field created by the Au NPs underneath can sufficiently penetrate the shell and enhance the fluorescence of the fluorophore immobilized therein. Moreover, a comparison material, 50 nm Au NPs, and the corresponding $Au_{55\ nm}@SiO_2$ NPs were synthesized (for details, see ESI, Fig. S1 and S2†).

Fig. 2a shows the UV-vis spectrum of the free fluorescent molecule, which exhibits a strong adsorption peak with a maximum wavelength (λ_{max}) of 563 nm. Upon the addition of Hg^{2+} ions, the λ_{max} red-shifts to 570 nm. At the same time, as shown in the corresponding fluorescence spectrum in Fig. 2b, the fluorescence intensity of the free fluorescent probe was enhanced after the addition of Hg^{2+}, indicating that the ring-opening reaction occurred in the fluorescent molecule. Interestingly, the fluorescence intensity was dramatically enhanced when Hg^{2+} was added to the solution of the probe-labeled-$Au@SiO_2$, which is because the excitation region of the probe is consistent with the plasmon of $Au@SiO_2$ (Fig. 2b). The enhancement factor therefore results from the mercury-induced ring-opening reaction. More importantly, MEF, as a leading effect, causes a significant fluorescence enhancement. Because of the much wider resonance, the enhancement effect of the probe-labeled $Au@SiO_2$ NPs is more remarkable than that of the free fluorescent probe. A comparison was made using 55 nm gold NPs, and it was found that the 80 nm NPs have better MEF performance (for details, see ESI, Fig. S3†). The time profile of the fluorescence response of the probes (0.5 μM) in the presence of Hg^{2+} (1.0 equiv.) in pH 7.4 PBS buffer is displayed in Fig. S4,† showing that the response of probes to sulfite was very quick. In addition, to study the stability of the probes at different pH values, the fluorescence spectra of the response of the probes toward Hg^{2+} under different pH conditions were evaluated (Fig. S5, see ESI†). These results clearly show that this probe can be used in a broad pH range of 6.0–9.0. This result shows that the probes can be applied to biological systems.

Fig. 3a and b show the fluorescence spectrum of the free fluorescent probe and fluorophore-labeled $Au@SiO_2$ probe, respectively, in the presence of different amounts of Hg^{2+} ions. For reliable comparison, the number of fluorescent probes

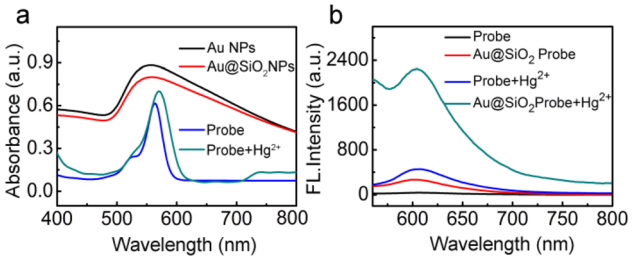

Fig. 2 (a) UV-vis spectra for 0.5 μM of the free fluorescent probe, $Au@SiO_2$ NPs, free fluorescent probe and fluorophore-labeled $Au@SiO_2$ probe with the addition of Hg^{2+}. (b) Fluorescence spectra of the free probe, fluorophore-labeled $Au@SiO_2$ probe, and corresponding changes in fluorescence intensity after the addition of Hg^{2+}. The concentration of the probe and Hg^{2+} are all 0.5 μM.

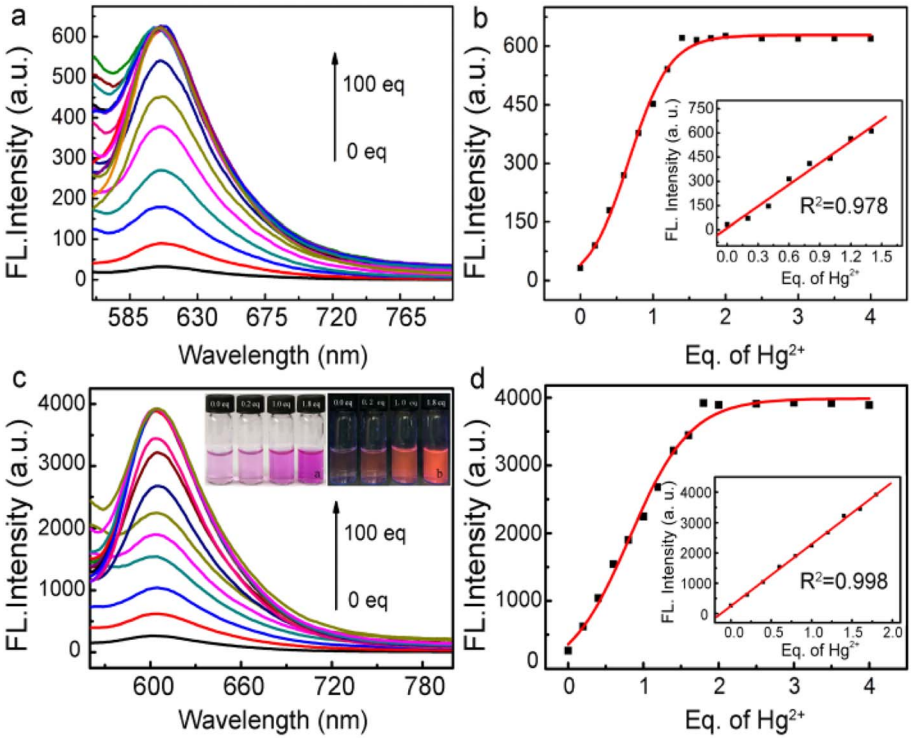

Fig. 3 (a) Fluorescence spectra of the free fluorescent probe (0.5 μM) in the presence of different amounts of Hg^{2+} ions and (b) fluorescence intensity as a function of the amount of Hg^{2+} ions and corresponding linearity in the inset. (c) Fluorescence spectra for the fluorophore-labeled Au@SiO_2 probe with various amounts of Hg^{2+}, and corresponding fluorescence images with various amounts of Hg^{2+} in the inset. (d) Change in fluorescence intensity as a function of Hg^{2+} ion concentration and the corresponding linearity in the inset. The final concentrations for both probes were 0.5 μM. Excitation at 560 nm.

immobilized on the Au@SiO_2 NPs was adjusted to the same amount (all achieved 0.5 μM). After that, Hg^{2+} ions were introduced with increasing molar ratio to the probe-labeled Au@SiO_2 NP solutions. With increasing amount of Hg^{2+} ions, the intensity of the fluorescence initially quickly increased. The fluorescence intensities then became saturated at a molar ratio of 1.8 for the probe-labeled Au@SiO_2 NPs and 1.4 for the free fluorescent probe, as shown in Fig. 3b and d, because the mercury-induced ring-opening reactions reached equilibrium. The addition of Hg^{2+} to the probe-labeled Au@SiO_2 solutions causes strong yellow fluorescence, as shown in the inset of Fig. 3c. Consistent with its large fluorescence enhancement ability (Fig. 3a and c), the fluorescence enhancement achieved on the Au@SiO_2 probe is more prominent than that achieved for the free fluorescent probes. The number of fluorescent molecules immobilized on the surface of the Au@SiO_2 NPs can be estimated, as described in the ESI Fig. S6† section;[52] the fluorescence enhancement achieved on the Au@SiO_2 NPs was 8.2-fold. With this core–shell type configuration, the fluorescence enhancement arises because the plasmon of the inner Au NPs is resonant with maximum UV-vis absorption peaks for the fluorescent probe. This large fluorescence enhancement makes the Au@SiO_2 NPs very attractive for the practical detection of Hg^{2+} ions, which relies on fluorescence as the signaling pathway. The plots shown in Fig. 3b and d reveal that the fluorescence intensities changed as a function of the Hg^{2+} concentration, and the insets show the linear plot ranges of fluorescence intensity *versus* Hg^{2+} ionic concentration that were extracted from Fig. 3b and d. For the free fluorescent probe (Fig. 3b), the detection limit achieved is 8.5×10^{-9} M, while that achieved for the Au@SiO_2 NPs is 5.0×10^{-11} M. The capability of our MEF probe to detect Hg^{2+} was comparable to that of other materials (Table 1). Apparently, owing to the large fluorescence enhancement, the fluorophore-labeled Au@SiO_2 probes show much improved sensitivity toward Hg^{2+} ions. To study the stability of the probe RS (Rhodamine spirocyclic type fluorescent molecular probe) at different pH values, the fluorescence

Table 1 Comparison of the limit of detection (LOD) for the Hg^{2+} ion detected using the fluorophore-labeled Au@SiO_2 probe and other fluorescent probes

Material	LOD/mol L^{-1}	Year	Ref.
SBA-15	0.6×10^{-6}	2008	53
$NaYF_4$:Yb^{3+}	0.6×10^{-10}	2010	54
CdTe QDs	0.7×10^{-7}	2012	55
Rhodamine derivative	2.9×10^{-8}	2013	56
Au NP	5.0×10^{-9}	2016	57
Aptamer-Ag@SiO_2	3.3×10^{-10}	2015	58
Unsymmetrical quinoline type tolans	2.0×10^{-10}	2016	59
G-quadruplex DNA	1.3×10^{-10}	2017	60
Au/N-CQDs	1.2×10^{-5}	2018	61
Ag@SiO_2 NPs	2.0×10^{-19}	2022	62
Au@SiO_2-probe	5.0×10^{-11}	Now	This work

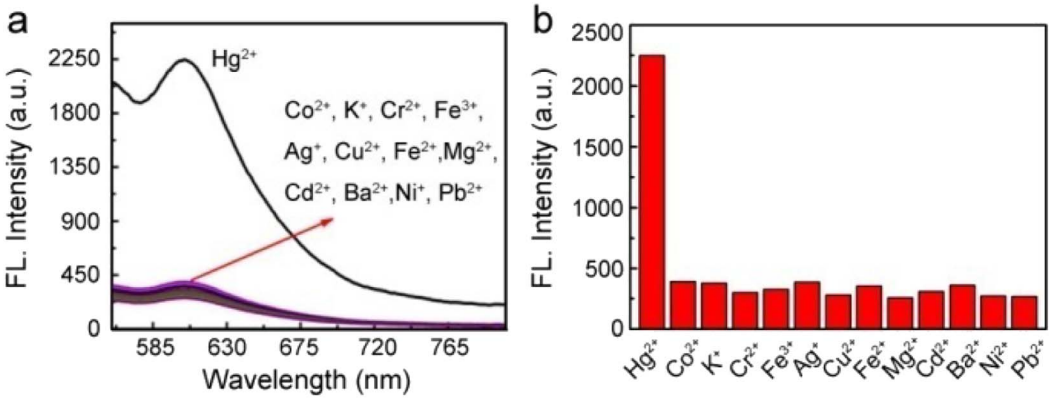

Fig. 4 (a) Fluorescence spectra for the fluorophore-labeled Au@SiO_2 probe in the presence of 1.0 equivalent of Hg^{2+}, Co^{2+}, Fe^{3+}, Cd^{2+}, Fe^{2+}, K^+, Cr^{2+}, Cu^{2+}, Pb^{2+}, Mg^{2+}, Ag^+, Ba^{2+}, and Ni^{2+}. The final concentration of the probe and metal ions are all 0.5 μM. (b) Selectivity of NP sensors plotted in histogram form.

spectra of the RS response toward Hg^{2+} under different pH conditions were evaluated (Fig. S5, see ESI†). These results clearly show that this probe can be used in a broad range pH of 6.0–9.0.

To further reveal their resistance against interferent ions, Fig. 4a and b shows fluorescence spectra for the Au@SiO_2 probes in the presence of other metal ions, namely, Co^{2+}, Fe^{3+}, Cd^{2+}, Fe^{2+}, K^+, Cr^{2+}, Cu^{2+}, Pb^{2+}, Mg^{2+}, Ag^+, Ba^{2+}, and Ni^{2+} ions. Clearly, only the presence of Hg^{2+} ions can trigger the high fluorescence intensity of the probe, thereby indicating the excellent selectivity of the Au@SiO_2 fluorescent probes. In addition, we further examined the fluorescence response of the probe toward Hg^{2+} ions in the presence of other potentially competing species. These other species only displayed minimum interference (Fig. S7†). This suggests that the Au@SiO_2 probe is potentially useful for sensing Hg^{2+} ions in the presence of other related species in pH 7.4 PBS buffer.

Because of the desirable sensitivity and selectivity of this fluorophore-labeled Au@SiO_2 probe toward Hg^{2+} ions, it shows potential application in real water sample analysis. For demonstration, the proposed fluorescent probe was applied to detect Hg^{2+} ions in many different kinds of water collected from local places (Xiangjiang River, Peach Lake, and Yuelu Mountain Spring, in Changsha, China). The fluorescence intensity of the solutions was recorded after adding the fluorophore-labeled Au@SiO_2 and a spiking concentration of Hg^{2+} ions to the water samples. To prove the reliability of our sensor, the same detection was carried out using ICP (inductive coupled plasma emission spectrometry), and the results are summarized in Table 2. The results of the two methods show good agreement between expected and found values, which proved that the Au@SiO_2 NP fluorescent probes exhibit satisfactory performances in real environmental water samples.

To demonstrate the potential use of the probe and Au@SiO_2 probe in bioimaging applications, we tested the cytotoxicity of the Au@SiO_2 probe toward HCT116 colorectal cancer cells using the reduction activity of the methylthiazolyltetrazolium (MTT) assay (Fig. S8, see ESI†). The viability of untreated cells was assumed to be 100%. Upon the incubation with 0.5 μM of the probe or Au@SiO_2 probe for 24 h, no significant difference in the proliferation of the cells was observed. Specifically, a cell viability of about 80% was observed after 24 h even at a high-

Table 2 Determination of Hg^{2+} ion content in real water samples using probes ($n = 3$)[a]

Sample	Added (equiv.)	Measured	ICP (mol L^{-1})
River water	0	N	N
	1.00	1.13	5.27×10^{-7}
	1.60	1.75	8.18×10^{-7}
Lake water	0	N	N
	1.00	1.32	5.41×10^{-7}
	1.60	1.94	8.33×10^{-7}
Spring water	0	N	N
	1.00	0.92	4.66×10^{-7}
	1.60	1.43	7.72×10^{-7}

[a] N = no Hg^{2+} was detected.

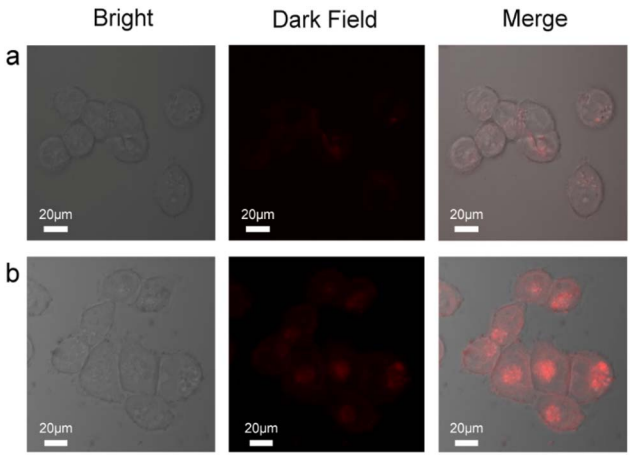

Fig. 5 Fluorescence microscopic images of HCT116 cells: (a) after treatment with 0.5 μM probe and the addition of 5 μM Hg^{2+} (under red light) to probe-treated cells. (b) After treatment with 0.5 μM Au@SiO_2 probe and the addition of 5 μM Hg^{2+} (under red light) to probe-treated cells.

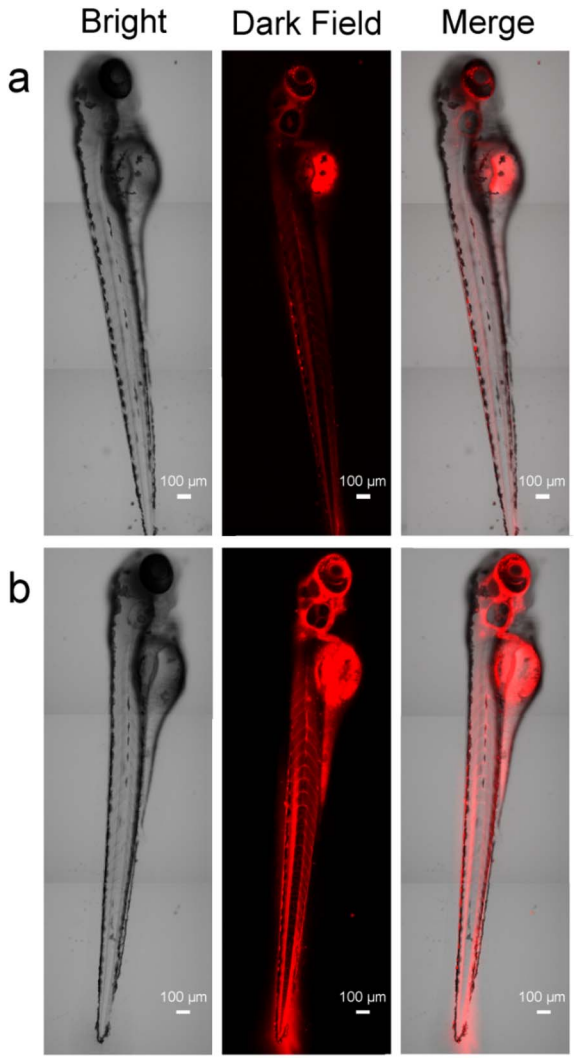

Fig. 6 Fluorescence microscopic images of three-day-old zebrafish incubated with probe (a) and Au@SiO_2 probe and (b) in the presence of Hg^{2+}. Bright field image (left), fluorescence image (middle), and merged image (right).

dose concentration of 1.8 equiv. Hg^{2+}. These data indicated the satisfactory biocompatibility of the Hg^{2+} fluorescent probe at all dosages, enabling the probe and Au@SiO_2 probe to serve as a potential probe for fluorescence bioimaging.

To extend the application of the probes to more complex metrics, we examined the imaging characteristics of the probes in cultured living cells *in vitro* (HCT116, human colorectal cancer cells) using fluorescence microscopy (Fig. 5). The cells were incubated with 0.5 μM of the probe and Au@SiO_2 probe for 1 h and 6 h at 37 °C, respectively. The cells were then washed with PBS three times and mounted on a microscope stage. As shown in Fig. 5a, the cells display modest intracellular staining after incubation with the probe and subsequent addition of 1.8 equiv. Hg^{2+}. Upon incubation for 1 h, striking turn-on fluorescence is observed inside the HCT116 cells, indicating the formation of the probe + Hg^{2+} complex, which was in agreement with studies performed in solution. Under same conditions, the Au@SiO_2 probe (0.5 μM) was incubated for 6 h and 1.8 equiv. Hg^{2+} was added and incubated for 1 h, and a notable enhancement was observed (Fig. 5b). In contrast, the Au@SiO_2 probe produces a stronger fluorescence imaging effect than the free probe. The fluorescence microscopy analysis strongly suggested that the Au@SiO_2 probe could cross the membrane barrier, permeate into the HCT116 cells, and rapidly sense intracellular Hg^{2+}. It is significant to mention that bright field imaging of treated cells did not reveal any gross morphological perturbations, which suggested that the HCT116 cells were viable. These preliminary experimental results demonstrated that the Au@SiO_2 probe could be applied for the fluorescence imaging of Hg^{2+} in biological samples with high resolution.

Whole-organism experiments were also carried out to examine whether the probe could be used to image Hg^{2+} in living organisms. A 3 day-old zebrafish was incubated with 1 μM of probe and Au@SiO_2 probe in E3 embryo media for 4 h and 24 h at 28 °C and later incubated in a solution containing 1.8 equiv. Hg^{2+} for 2 h. Subsequently, the samples were washed with PBS to remove remaining probes. The treated zebrafish is shown in Fig. 6. The zebrafish remained alive throughout imaging experiments. The results of fluorescence microscopy analysis of these specimens showed that Hg^{2+} in the zebrafish was fluorescently detected by the probes (Table 1). In this case, the Au@SiO_2 probe has stronger fluorescence intensity than the free probe. These results indicate that the probes are useful for the study of the toxicity or bioactivity of Hg^{2+} in living organisms.

Experimental

Materials and methods

Sodium silicate solution (≥27 wt% SiO_2), 3-aminopropyltrimethoxysilane (APTS, 97%), and chloroauric acid (≥99.9%) were obtained from Sigma-Aldrich, Alfa Aesar, and Jiuyue Chemical Ltd Co. (Shanghai, China), respectively. Sodium citrate, hydrochloric acid, mercuric nitrate ($Hg(NO_3)_2$), phosphate buffer saline (PBS), ethanol, and dimethyl formamide (DMF), all of analytical grade, were purchased from Sinopharm Chemical Reagent Ltd Co. (Shanghai, China). DMEM (Dulbecco's Modified Eagle Medium) were purchased from Sangon Biotech Reagent Ltd Co. (Shanghai, China). Other materials were obtained from native suppliers (Changsha Longhe Chemical and Glass Experimental Products Ltd Co. (Changsha, China)), and all materials were used as received without further purification.

Synthesis of Au@SiO_2 core–shell NPs

The synthesis of the Au@SiO_2 core–shell NPs involves the preparation of the Au NPs and subsequent silica coating.[51] In brief, 80 nm (in diameter) Au NPs were synthesized following Frens's method.[63] After that, freshly prepared APTS solution (0.63 mL, 1 mM) and as-synthesized 80 nm Au colloids (90 mL) were mixed at room temperature, followed by vigorous stirring for 15 min. To the above mixture was then added activated sodium silicate solution (6.3 mL, 0.54 wt%). Prior to use, the silica solution was activated by adjusting its pH to 10.2–10.3 using 0.5 M HCl solution. After stirring for 3 min,

aforementioned mixtures were transferred into a 95 °C water bath and stirred at this temperature for another 1 h to accomplish the silica coating. The final Au@SiO_2 NPs were collected by centrifugation at 2500 rpm and stored in water (20 mL).

Examining the coating quality of the synthesized Au@SiO_2 NPs

The coating quality of the SiO_2 shell on the Au nanoparticles (NPs) was examined using cyclic voltammetry (CV) and surface-enhanced Raman scattering (SERS) studies.[51] For CV measurements, the working electrode was prepared by drying concentrated dispersions of Au NPs or Au@SiO_2 NPs (40 mL, concentrated from 4 mL original colloids) on a glass carbon (GC) electrode (3 mm, in diameter). The CV curves for the Au NPs and Au@SiO_2 NPs were measured in 0.5 M H_2SO_4 solution. For SERS measurements, a drop of the concentrated dispersion of Au@SiO_2 NPs was dried on a Si wafer, onto which was spread a drop of 0.001 M pyridine solution; the wafer was then covered with a cover glass to prevent water evaporation.

Fluorescence labeling of the Au@SiO_2 NPs

The fluorescent probe, 2,5-dioxopyrrolidin-1-yl-4-(3-(3′,6′-bis(diethylamino)-3-oxospiro[isoindoline-1,9′-xanthen]-2-yl)thioureido) benzoate was synthesized according to a literature report.[20] Prior to use, the fluorescent probe was dissolved in a mixed solution of PBS and ethanol (v:v, 7 : 3) with pH = 7.4. To immobilize the fluorescent probe onto the Au@SiO_2 NPs, APTS was used as the linker.[64] Briefly, freshly prepared APTS solution (1.12 mL, 1 mM) was added to a dispersion of Au@SiO_2 NPs (4 mL) with vigorous stirring and were stirred for 15 min. The residual, unlinked APTS was removed by centrifugation/re-dispersion of the above mixtures in DMF three times, and the collected Au@SiO_2 NPs were redispersed in DMF (20 mL). After that, the fluorescent probe solution (4.26 mL, 5 μM) was added to the DMF dispersion of the Au@SiO_2 NPs and stirred in the dark and at room temperature for 24 h.[65] The fluorescent probe was immobilized onto the surface of the Au@SiO_2 NPs by the amidogen of APTS reacting with the ester group of the fluorescent probe. The fluorescent-probe-labeled Au@SiO_2 NPs were collected by centrifugation, washed with ethanol and PBS/ethanol (v/v, 7/3) solution twice each, and re-dispersed in PBS/ethanol solution (10 mL).

Fluorescence detection of Hg^{2+} ion

To test Hg^{2+} ions, the probe-labeled Au@SiO_2 NP dispersion (254 μL, 0.98 μM) was placed into 2 mL test tubes, followed by the addition of a certain amount of Hg^{2+} ions ($Hg(NO_3)_2$ in PBS/ethanol solution). For all these measurements, the final probe concentration in the solution was 0.5 μM, with the molar ratio of Hg^{2+} ion to probe varying from 0 to 100.0. After the addition of Hg^{2+} ions, the solutions were allowed to stand undisturbed at room temperature for 2 h, followed by fluorescence measurement. For comparison, the fluorescence detection of other interferent ions ($CoCl_2$, $FeCl_3$, $CdCl_2$, $FeSO_4$, KCl, $Cr(NO_3)_2$, $CuCl_2$, $Pb(NO_3)_2$, $MgCl_2$, $AgNO_3$, $BaCl_2$ and $Ni(NO_3)_2$ in PBS/ethanol solution) was similarly tested using the fluorescent-probe-labeled Au@SiO_2 NPs at a resultant concentration of 0.5 μM for the fluorescent probe and a 1.0 molar ratio of the different ions.

Analysis of real water samples

To evaluate the practical potential of the Au@SiO_2 NPs fluorescent probe, it was also used for the detection of Hg^{2+} ions in real water samples. Three real water samples were taken from Xiang River, Peach Lake, and Yuelu Mountain Spring (Changsha, China). Before measurements, the water samples were filtered through a 0.22 μm membrane syringe filter to filter out impurities. Then, 254 μL of the Au@SiO_2 NPs fluorescent probe solution was dropped into the water sample. Subsequently, Hg^{2+} solutions were added to the Au@SiO_2 NRs/water system at a final concentration of 0, 100, or 200 nM, and the water samples were then determined using fluorescence and ICP-MS.

Cell cultures

The human colorectal cancer cell line HCT116 cells were provided by the Institute of Biochemistry and Cell Biology, Hunan University (Changsha, China). The cells were propagated in Dulbecco's Modified Eagle's Medium (DMEM) supplemented with 10% (v/v) fetal bovine serum, penicillin (100 μg mL^{-1}), and streptomycin (100 μg mL^{-1}). Cells were maintained under a humidified atmosphere of 5% CO_2 and at 37 °C in an incubator as mentioned before.

Cytotoxicity of the Au@SiO_2 probe

The cytotoxic effect of the Au@SiO_2 probe was determined using an MTT assay following manufacturer's instructions (Sigma-Aldrich, MO). Human colorectal cancer cell line HCT116 cells, provided by the Institute of Biochemistry and Cell Biology, Hunan University (Changsha, China), were seeded in a 96-well plate (2000 cells per well) with DMEM in an atmosphere of 5% CO_2 and 95% air at 37 °C for 24 h. Then, the cells were incubated with DMEM containing various concentrations of the Au@SiO_2 probe with different final concentrations (0.5, 1, 3, 5, 10 and 20 μM), while some cells were treated with $Hg(NO_3)_2$ (0.9 μM) alone. The cells were then incubated at 37 °C in an atmosphere of 5% CO_2 and 95% air at 37 °C for 24 h, followed by MTT assays. An untreated assay with DMEM ($n = 3$) was also conducted under same conditions.

Cell imaging experiments

For cell imaging studies, cells were seeded into a confocal dish and incubated at 37 °C in a CO_2 incubator for 2 h. After one day, the cells were washed three times with phosphate buffered saline (pH 7.4) and incubated with 0.5 μM probe or Au@SiO_2 probe in DMEM at 37 °C for 1 h and 6 h in a CO_2 incubator and later incubated in DMEM with 1.8 equiv. $Hg(NO_3)_2$ for 1 h. The cells were again washed thrice with PBS (pH 7.4) to remove the probe or Au@SiO_2 probe. Finally, the samples were observed under a TI-E + A1 SI Nikon laser confocal microscope and images were taken.

Imaging of zebrafish

Zebrafish were obtained from the School of Life Sciences of Hunan Normal University (Changsha, China). The zebrafish were maintained in E3 embryo media (15 mM NaCl, 0.5 mM KCl, 1.0 mM $MgSO_4$, 1.0 mM $CaCl_2$, 0.15 mM KH_2PO_4, 0.05 mM

Na_2HPO_4, 0.7 mM $NaHCO_3$, and 5–10% methylene blue, pH 7.5). In fluorescence imaging experiments, three-day-old zebrafish were incubated with 1 μM probe and Au@SiO_2 probe in E3 embryo media for 4 h and 24 h at 28 °C and later incubated in a solution containing 1.8 equiv. Hg^{2+} for 1 h at 28 °C, respectively. Subsequently, the samples were washed with PBS to remove remaining probes and examined using a TI-E + A1 SI Nikon laser confocal microscope.

Characterization

UV-vis spectra and transmission electron microscopy (TEM) images were obtained using a UV-1800 spectrophotometer using 1 cm quartz cells (Shimadzu, Japan) and a JEM-2100F microscope (JEOL, Japan), respectively. For TEM characterization, the samples were prepared by drying a drop of dilute particle dispersion on a carbon-coated Cu grid. Fluorescence spectra were measured using a F-4600 fluorescence spectrophotometer (Hitachi, Tokyo, Japan) under the excitation of a 560 nm laser. Confocal laser scanning microscopy images were recorded on a TI-E + A1 SI, Nikon.

Conclusions

In conclusion, we have developed a highly sensitive and selective metal-enhanced fluorescence chemodosimeter for the detection of Hg^{2+} ions, prepared by the immobilization of "turn-on" fluorescent probes on Au@SiO_2 NPs. With this configuration, the chemodosimeter Au@SiO_2 probe with an 80 nm core can produce an 8.2-fold fluorescence enhancement, while the thin SiO_2 shell effectively prevents fluorescence quenching. The optimized detection limit achieved was 5.0×10^{-11} M, which was about two orders of magnitude lower than that achieved using the free fluorescent probe (8.5×10^{-9} M) and far lower than the permissible EPA limit of Hg^{2+} ions in drinkable water (<10 nM). These results suggest that the fluorophore-labeled Au@SiO_2 probe has great potential for practical detection of Hg^{2+} ions in the environment, food samples, and even whole cells.

Author contributions

Ying Cui and Shanji Fan contributed equally to this work. Ying Cui, conceptualization, methodology, investigation, writing – original draft, Shanji Fan, conceptualization, methodology, writing original draft, funding acquisition, review & editing, Yunran Zhai, investigation, Yingjie Liu, investigation, Junhua Li, review & editing, Jiawen Hu, methodology, writing, review & editing, Lijia Wang, methodology, writing, review & editing, funding acquisition, supervision.

Conflicts of interest

There are no conflicts to declare.

Acknowledgements

This research work was supported by Hunan Provincial Natural Science Foundation of China (Grant No. 2022JJ40393 and 2023JJ50093), Zhejiang Provincial Natural Science Foundation of China (Grant No. LBY22H180013), Science Foundation of Hengyang Normal University of China (No. 2021QD03), Hengyang Normal University Industrial Supported Project (No. HXKY2023042), Key Laboratory of Functional Metal-Organic Compounds of Hunan Province of Hengyang Normal University (Grant No. 2023HSKFJJ007), and Hunan Provincial Health Commission Research (Grant No. 202204014247). This research work was also supported by Medical and Health Science and Technology Program of Zhejiang Province (Grant No. 2021RC085).

Notes and references

1 J. O. Nriagu, *Nature*, 1979, **279**, 409–411.
2 G. Cabana and J. B. Rasmussen, *Nature*, 1994, **372**(6503), 255–257.
3 T. W. Clarkson, L. Magos and G. J. Myers, *N. Engl. J. Med.*, 2003, **349**(18), 1731–1737.
4 A. Renzoni, F. Zino and E. Franchi, *Environ. Res.*, 1998, **77**(2), 68–72.
5 U. EPA, *National Primary Drinking Water Regulations, Arsenic and Clarifications*, 2009.
6 O. Caylak, S. G. Elci, A. Hol, A. Akdogan, U. Divrikli and L. Elci, *Food Chem.*, 2019, **274**, 487–493.
7 F. M. Teeny, *J. Agric. Food Chem.*, 1975, **23**(4), 668–671.
8 F. X. X. Han, W. D. Patterson, Y. J. Xia, B. B. Sridhar and Y. Su, *Water, Air, Soil Pollut.*, 2006, **170**(1–4), 161–171.
9 J. Mo, Q. Li, X. Guo, G. Zhang and Z. Wang, *Anal. Chem.*, 2017, **89**(19), 10353–10360.
10 V. L. Dressler, F. G. Antes, C. M. Moreira, D. Pozebon and F. A. Duarte, *Int. J. Mass Spectrom.*, 2011, **307**(1–3), 149–162.
11 C. D. Palmer, M. E. Lewis, C. M. Geraghty Jr, F. Barbosa Jr and P. J. Parsons, *Spectrochim. Acta, Part B*, 2006, **61**(8), 980–990.
12 O. T. Butler, W. R. L. Cairns and J. M. Cookc, *J. Anal. At. Spectrom.*, 2017, **32**(1), 11–57.
13 Y. Yin, J. Liu and G. Jiang, *Chin. Sci. Bull.*, 2013, **58**(2), 150–161.
14 Q. Lin, P. Chen, J. Liu, Y. Fu, Y. Zhang and T. Wei, *Prog. Chem.*, 2013, **25**(7), 1177–1186.
15 E. M. Nolan and S. J. Lippard, *J. Am. Chem. Soc.*, 2003, **125**(47), 14270–14271.
16 M. Y. Chae and A. W. Czarnik, *J. Am. Chem. Soc.*, 1992, **114**, 9704–9705.
17 Y. Xu, Z. Jiang, Y. Xiao, T. T. Zhang, J. Y. Miao and B. X. Zhao, *Anal. Chim. Acta*, 2014, **807**, 126–134.
18 M. G. Choi, H. G. Im, J. H. Noh, D. H. Ryu and S. K. Chang, *Sens. Actuators, B*, 2013, **177**, 583–588.
19 A. K. Manna, J. Mondal, R. Chandra, K. Rout and G. K. Patra, *J. Photochem. Photobiol., A*, 2018, **356**, 477–488.
20 Y. K. Yang, K. J. Yook and J. Tae, *J. Am. Chem. Soc.*, 2005, **127**(48), 16760–16761.
21 K. H. Drexhage, *J. Lumin.*, 1970, **1–2**, 693–701.
22 Y. Jeong, Y. M. Kook, K. Lee and W. G. Koh, *Biosens. Bioelectron.*, 2018, **111**, 102–116.

23 H. Pei, S. Zhu, M. Yang, R. Kong, Y. Zheng and F. Qu, *Biosens. Bioelectron.*, 2015, **74**, 909–914.
24 Z. Zhou, H. Huang, Y. Chen, F. Liu, C. Z. Huang and N. Li, *Biosens. Bioelectron.*, 2014, **52**, 367–373.
25 H. Wang, T. Kang, X. Wang and L. Feng, *Sens. Actuators, B*, 2018, **264**(3), 391–397.
26 X. Wang, L. Liu, S. Zhu and L. Li, *Phys. Status Solidi RRL*, 2019, **13**(2), 1800521.
27 C. Li, Y. Zhu, X. Zhang, X. Yang and C. Li, *RSC Adv.*, 2012, **2**(5), 1765–1768.
28 C. Zhai, Z. Chen, S. Lv, Y. Lin, Z. Zhang and D. Pang, *Prog. Chem.*, 2017, **29**(8), 814–823.
29 J. R. Bhamore, Z. V. P. Murthy and S. K. Kailasa, *J. Mol. Liq.*, 2019, **280**, 18–24.
30 A. I. Dragan, E. S. Bishop, J. R. Casas-Finet, R. J. Strouse, J. McGivney, M. A. Schenerman and C. D. Geddes, *Plasmonics*, 2012, **7**, 739–744.
31 H. I. Peng, C. M. Strohsahl, K. E. Leach, T. D. Krauss and B. L. Miller, *ACS Nano*, 2009, **3**, 2265–2273.
32 K. Aslan, R. Badugu, J. R. Lakowicz and C. D. Geddes, *J. Fluoresc.*, 2018, **15**(2), 99–104.
33 V. Srinivasan, A. U. Andar, Y. Kostov and G. Rao, *Plasmonics*, 2019, **14**(3), 731–736.
34 Y. Zhang, K. Aslan, M. J. R. Previte and C. D. Geddes, *Dyes Pigm.*, 2008, **77**, 545–549.
35 G. Hong, S. M. Tabakman, K. Welsher, H. Wang, X. Wang and H. Dai, *J. Am. Chem. Soc.*, 2010, **132**, 15920–15923.
36 L. Jiang, X. Hang, P. Zhang, J. Wang, Y. Wang and L. Ren, *Microchem. J.*, 2019, **148**, 285–290.
37 A. V. Veglia and A. Guillermo Bracamonte, *J. Nanophotonics*, 2018, **12**(3), 033004.
38 K. Aslan, M. Wu, J. R. Lakowicz and C. D. Geddes, *J. Am. Chem. Soc.*, 2007, **129**(6), 1524–1525.
39 I. G. Theodorou, Q. Jiang, L. Malms, X. Xie, R. C. Coombes, E. O. Aboagye, A. E. Porter, M. P. Ryan and F. Xie, *Nanoscale*, 2018, **10**(33), 15854–15864.
40 C. Joyce, S. M. Fothergill and F. Xie, *Mater. Today Adv.*, 2020, **7**, 100073.
41 Z. Shen, C. Zhang, X. Yu, J. Li, Z. Wang, Z. Zhang and B. Liu, *J. Mater. Chem. C*, 2018, **6**(36), 9636–9641.
42 H. Jiang, D. Tang, Z. J. Li, J. W. Li, H. B. Liu, Q. J. Meng, Q. X. Han and X. A. Liu, *Spectrochim. Acta.A.*, 2020, **243**, 118784.
43 A. Caballero, R. Martinez, V. Lloveras, I. Ratera, J. Vidal-Gancedo, K. Wurst, A. Tarraga, P. Molina and J. Veciana, *J. Am. Chem. Soc.*, 2005, **127**(45), 15666–15667.
44 V. Narayanan, V. Ganesan, E. Shanmugasundram, S. Durganandini, K. Vellaisamy, H. Amirthalingam and S. Thambusamy, *J. Photochem. Photobiol., A*, 2023, **445**, 115069.
45 G. G. Talanova, N. S. Elkarim, V. S. Talanov and R. A. Bartsch, *Anal. Chem.*, 1999, **71**, 3106–3109.
46 Z. Cheng, G. Li and M. Liu, *J. Hazard. Mater.*, 2015, **287**, 402–411.
47 S. Ishida, D. Kitagawa, S. Kobatake, S. Kim, S. Kurihara and T. Fukaminato, *Chem. Commun.*, 2019, **55**, 5681–5684.
48 Y. Pang, Z. Rong, R. Xiao and S. Wang, *Sci. Rep.*, 2015, **5**, 11005–11012.
49 Y. P. Li, X. H. Zhu, S. N. Li, Y. C. Jiang, M. C. Hu and Q. G. Zhai, *ACS Appl. Mater. Interfaces*, 2019, **11**(12), 11338–11348.
50 Y. P. Li, X. H. Zhu, S. N. Li, Y. C. Jiang, M. C. Hu and Q. G. Zhai, *ACS Appl. Mater. Interfaces*, 2019, **11**, 11338–11348.
51 J. F. Li, Y. F. Huang, Y. Ding, Z. L. Yang, S. B. Li, X. S. Zhou, F. R. Fan, W. Zhang, Z. Y. Zhou, D. Y. Wu, B. Ren, Z. L. Wang and Z. Q. Tian, *Nature*, 2010, **464**(7287), 392–395.
52 J. Peng, W. Xu, C. L. Teoh, S. Han, B. Kim, A. Samanta, J. C. Er, L. Wang, L. Yuan, X. Liu and Y. T. Chang, *J. Am. Chem. Soc.*, 2015, **137**, 2336–2342.
53 J. Wang, H. Li, X. Min, L. Long, W. Ying, G. Ling, J. Zhu and Z. Zou, *Appl. Surf. Sci.*, 2008, **254**(17), 5329–5335.
54 M. Kumar and P. Zhang, *Biosens. Bioelectron.*, 2010, **25**(11), 2431–2435.
55 J. Pei, H. Zhu, X. Wang, H. Zhang and X. Yang, *Anal. Chim. Acta*, 2012, **757**, 63–68.
56 X. Zhou, W. Yan, T. Zhao, Z. Tian and X. Wu, *Tetrahedron*, 2013, **69**(46), 9535–9539.
57 J. Li, J. Chen, Y. Chen, Y. Li and C. Yu, *Analyst*, 2015, **141**(1), 346.
58 Y. Pang, Z. Rong, R. Xiao and S. Wang, *Sci. Rep.*, 2015, **5**, 9451.
59 J. H. Hong, S. Kurapati, Y. Jo, J. H. Shin and D. G. Cho, *Chem. Commun.*, 2016, **52**(71), 10759–10762.
60 X. Zhang, B. Ding, W. U. Hua, J. Wang and H. A. Yang, *Anal. Sci.*, 2017, **33**(2), 165–169.
61 A. Meng, Q. Xu, K. Zhao, Z. Li, J. Liang and Q. A. Li, *Sens. Actuators, B*, 2018, **255**(1), 657–665.
62 A. Picard-Lafond, D. Larivière and D. Boudreau, *ACS Omega*, 2022, **7**(26), 22944–22955.
63 G. Frens, *Nat. Phys. Sci.*, 1973, **241**(105), 20–22.
64 R. Bardhan, N. K. Grady and N. J. Halas, *Small*, 2008, **4**, 1716–1722.
65 A. Kaur, M. A. Haghighatbin, C. F. Hogan and E. J. New, *Chem. Commun.*, 2015, **51**, 10510–10513.